Eu$_2$O$_3$ role in the optical and photoluminescence properties of 50 SiO$_2$ − 7 MgO − 20 ZnO − (23 − x) La$_2$O$_3$ − x Eu$_2$O$_3$ nano-crystalline thin films

A. Dahshan[1,2] · Ali B. Abou Hammad[3] · K. A. Aly[4,5] · Amany M. El Nahrawy[3]

Abstract

Nano-crystalline 50 SiO$_2$ − 7 MgO − 20 ZnO − (23 − x) La$_2$O$_3$ − xEu$_2$O$_3$(0.0 ≤ x ≤ 4 mol%.) termed as (Eu-SMZL) thin films have been synthesized by highly acidic sol–gel technique and calcined at 450 °C for 2 h. The nano-porous Eu-SMZL films showed the improved structure and morphology with increasing Eu$_2$O$_3$ content. The XRD and FTIR investigation proved an increase in the crystallinity and changes in the internal structure with the increase in Eu^{3+} level. The photoluminescence (Pl) result agrees with the XRD, proving the increase in the crystallinity. The transmittance (T) and absorbance (A) spectra have been measured within 300–2000 nm spectral range. The absorption coefficient (α) and refractive index (n) have been estimated. It is worth to mention that the increment of Eu$_2$O$_3$ at the expense of La$_2$O$_3$ shifts the absorption edge to the long wavelength side (red shift) which leads to a decrement in the band gap (E_{opt}) values while the n values increases. This behavior of n is well discussed in terms of the glass density (G_d), molar volume (V_m), electronic polarizability (α_{el}) and optical basicity (Λ). Furthermore, the single oscillator model helps us to investigate the static index of refraction ($n(0)$), energy of single oscillator (E_o), and dispersion energy (E_d).

1 Introduction

A considerable attention has been paid to trivalent lanthanide-doped materials due to their uses in many applications as fiber amplifiers, solid-state laser, infrared–visible step-up transformers, phosphorescence, and field emission displays [1–4]. In this situation, glasses are the most investigated host materials due to their ease of fabrication, to add active ions with different amounts, and the potency to easily obtain bulk samples in comparison with single crystalline matrices. The main constructing bulk is tetrahedral SiO$_4$ units, and in pure SiO$_2$, all oxygen atoms will be divided between two tetrahedra pointing a totally polymerized network. Earth cations (alkali or alkaline) rule as network modifiers, fracturing the bridging oxygens (BOs) bond to form non-bridging oxygens (NBOs) as well as mollify in sites interesting to the tetrahedral network in nearby negatively charged NBOs [5]. The glass formation and structure are affected by the MgO concentration. Thus, Mg^{2+} is an important component of the mica structure [6]. Glass properties can be interpreted in terms of network connectivity (NC). The latter is the ratio between the number of bridging oxygen atoms (BO) and the network forming elements [7]. Therefore, pure silica glasses have an NC equal to 4, while a glass structure consisting of linear $\left(\text{SiO}_3\right)_n^{2n-}$ chains has an NC equal to 2. NC can be used to foresee surface reactivity, solubility or the likelihood of sustaining glass-in-glass phase separation and bioactivity [3]. Synthesis of trivalent lanthanide-doped silicate matrices, the class of the most attractive glass–ceramic system, has attracted obvious attention over the past decades, because of its high transparency, low thermal expansion coefficient and excellent chemical durability [1–3]. Sol–gel routes are well-established methods for high-purity synthesizing, ultra-fine particles, high surface area, single and complex

✉ A. Dahshan
adahshan73@gmail.com

1 Department of Physics, Faculty of Science, King Khalid University, P.O. Box 9004, Abha, Saudi Arabia

2 Department of Physics, Faculty of Science, Port Said University, Port Said, Egypt

3 Solid State Physics Department, Physics Research Division, National Research Centre, 33 El-Bohouth St., Dokki, Giza 12622, Egypt

4 Physics Department, Faculty of Science and Arts, Khulais, University of Jeddah, Jeddah, Saudi Arabia

5 Physics Department, Faculty of Science, Al-Azhar University, Assiut Branch, Assiut, Egypt

oxide glasses and ceramics with the characteristics of high homogeneity, low-temperature processing, high purity, and are cost-effective and environmentally friendly [8, 9]. Here, $50\, SiO_2 - 7\, MgO - 20\, ZnO - (23 - x)\, La_2O_3 - x\, Eu_2O_3$ $(0.0 \leq x \leq 4\, mol\%.)$ thin films were prepared following the acidic sol–gel route starting with hydrolyzed metal alkoxide (tetraethyl-orthosilicate (TEOS) with EtOH/H_2O/ HCL and aqua base for zinc, magnesium, lanthanum and europium nitrate solutions [10, 11]. The main aim of the present investigation is to study the effect of doping of Eu_2O_3 on silicate-based glasses, mainly their structural and optical characteristics.

2 Experimental work

2.1 Materials

Tetraethyl-orthosilicate (TEOS) 99.999%, magnesium-nitrate-hexahydrate ($Mg(NO_3)_2 \cdot 6H_2O$), zinc acetate dihydrate (($CH_3CO_2)_2Zn$, 99.99%), lanthanum (III) nitrate hydrate ($La(NO_3)_3 \cdot xH_2O$, 99.9%), europium(III) nitrate pentahydrate ($Eu(NO_3)3 \cdot 5H_2O$, 99.9%), hydrochloric acid (37%) and absolute ethanol (EtOH, 99.5%) were taken from Sigma (Aldrich), as starting materials for sensitization of (SMZL) and (Eu-SMZL) films.

2.2 Sensitization of nano-crystalline Eu-SMZL thin films

Facile sol–gel mechanisms were used for the preparation of $50\, SiO_2 - 7\, MgO - 20\, ZnO - (23 - x)\, La_2O_3 - x\, Eu_2O_3$ $(0.0 \leq x \leq 4\, mol\,\%)$ samples. The silica-based sol is formed by mixing (10 mL) TEOS/ (20/40 mL) of EtOH/ H_2O with drops of (HCL) as a catalyst. HCL was added to the solution under magnetic stirring at 50 °C as previously reported [12, 13]. Magnesium, zinc, and lanthanum solutions were added to the silica sol as a modifier. Second, for the preparation of (Eu-SMZL) sols, two stages were followed: (1) preparation of SMZ sol as described in the first step and (2) preparation of lanthanum sol doped with different concentrations (0–4 mol%) of europium sol and incorporating in (SMZ) according to their stoichiometric compositions. Films are termed approving to their Eu^{3+} level in La^{3+} sol, i.e., 0, 1, 2, 3, 4 Eu. After 2 h of mixing at 50 °C, the different sols for pure (SMZL) and Eu-SMZL were deposited on glass substrates (0.01 m × 0.02 m) by spin coating. The glass substrate was weaved 20 s subsequently after the sol was deposited on the substrate. The rate of spinning was 3000 rpm for 30 s. The sensitized films were desiccated at 40 °C for 24 h, and then calcined to 200 °C for 2 h to eliminate the residual solvents. Lastly, the prepared pure and doped SMZL thin films were calcined at 450 °C for 4 h in air.

2.3 Characterization techniques

Bruker D8 focus X-ray Diffractometer, from Germany equipped with CuKα ($\lambda = 1.54$ nm), has been used to characterize the sensitized films in the 2θ range of 10°–80°. The existence of different phases has been identified by using JCPDS data files in Pcpdfwin software.

The surface morphology of the films was analyzed using scanning electron microscopy (FE-SEM) (JSM 6360LV, JEOL/Noran). The images were obtained using an accelerating voltage of 15 kV. The two samples were analyzed by dispersing HF-etched calcined powders in absolute ethanol and setting drop-wise on copper grids that had previously been coated with a thin carbon film.

PerkinElmer C92035 spectrometer was used to investigate the Fourier-transform infrared (FTIR) spectra of the prepared films. The photoluminescence spectra were registered by [SPEX:750 M] monochromator equipped with a (Jobin Yvon/CCD-2000 800–3), in the Vis-range 400–850 nm, using (488 nm) argon-ion laser line, with error ratio $\pm$ 5 nm. The absorption spectra have been investigated over the wave number range of 1300–400 cm^{-1}. The optical absorption/ transmission spectra measurements have been carried out using Jasco V-570 spectrophotometer over the wavelength range, 0.2–2.5 μm, with error ratio $\pm$ 15.

3 Results and discussion

3.1 Phase purity

The X-ray diffraction (from $2\theta = 10°$ to 80°), calcined at 450 °C, confirms the crystalline structure of 50 SiO_2:7 MgO: 20 ZnO: (23−x) La_2O_3: x Eu_2O_3 (x=0, 1, 2, 3 and 4 mol%) (see Fig. 1). From XRD spectrum of (SMZL), all diffracted peaks represent orthorhombic phase of silica-magnesium-zinc (Si_2MgZnO_6, JCPDS-70-0853). With the addition of Eu_2O_3, a crystalline phase identified by monoclinic europium-silicate (Eu_2SiO_4, JCPDS-73-1156) nanoparticles due to the incorporation of Eu^{3+} in the silicate network is formed. Hence, the creation of an open silicate structure by introducing different modifiers, such as Zn, Mg and La, facilitates the interaction between SiO_2-network and the interacting Eu^{3+} as an active ion. The average crystallite size of the crystalline (SMZL-Eu^{3+}) thin films was 21–25 nm with increasing Eu^{3+} level, which was determined by Scherrer relation [14].

3.2 FE-SEM

Both pure and doped samples were calcined at 450 °C, as shown in Fig. 2, in which nano-crystalline particles
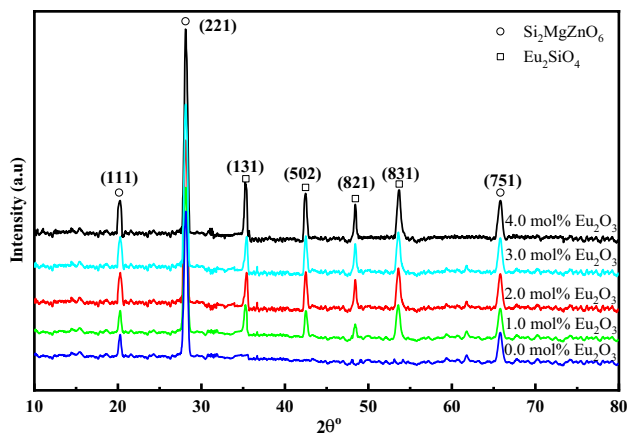
Fig. 1 XRD diffraction patterns of SMZL and doped with 1, 2, 3 and 4 mol% Eu$_2$O$_3$ ions nano-crystalline films

are already formed, and the nano-crystals of Eu^{3+} are engrossed in the (SMZL) phase. By introducing (4 mol%) Eu^{3+} ions, nano-crystals grow strongly at 450 °C and have a well-extended arrangement of formed (SMZL) film containing Eu^{3+} nano-crystals in their network, as shown in Fig. 2b. From FE-SEM images, it is noted that the prepared nano-crystalline films contain a cracking surface in some parts, which be due to the HF used for etching the films from the substrates.

3.3 FTIR study

FTIR spectra of nano-crystalline SMZL films doped with (2, 4 mol%) Eu^{3+} ions, calcined at 450 °C, display the fingerprint FTIR spectra for sol–gel silicate; the two absorption bands at 461 and 1107 cm^{-1} have been attributed to the binding and stretching vibration of Si–O–Si bonds as a basic bond with Zn–O–, La–O– and Mg–O– in the SiO$_4$ units, respectively [15, 16]. As shown in Fig. 3, the band at 797 cm^{-1} and the weak band at 971 cm^{-1} are the characteristics of the modified silicate glasses and are attributed to the vibrations of SiO^4 tetrahedral crosslinking with the Zn, M, La and Eu through oxygen bonds [17]. The absorption band at 1635 cm^{-1} is ascribed to interstitial H$_2$O, which bonded hydroxyl in the silicate network [13, 15].

3.4 Visible photoluminescence

Photoluminescence of emission spectra of (2–4 mol%) Eu^{3+}-SMZL nano-crystalline films has a red shift as indicated in Fig. 4. The intensity of emission peaks increased with increasing the Eu^{3+} content in SMZL. So, the increment in the emission shows three different peaks for the Eu^{3+} ions in the (SMZL) with increasing Eu^{3+} content. Hence, these visible transitions are sensitive to the internal changes in the surrounding ions, for (SMZL) matrix. Therefore, there is an obvious change in the peak intensity of the sensitive transition, due to the changes in the local symmetry of Eu^{3+}-doped ions. The direct or indirect (f–f) transitions of Eu^{3+} within
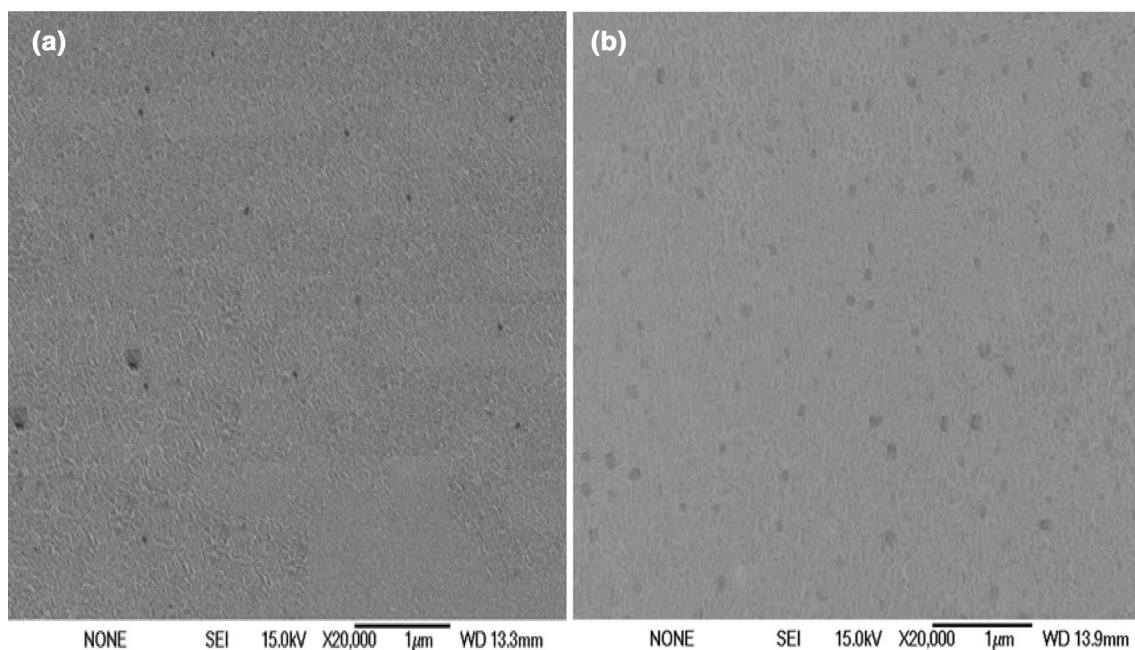

Fig. 2 SEM images of **a** SMZL, **b** doped with 4 mol% Eu$_2$O$_3$ ions nano-crystalline films
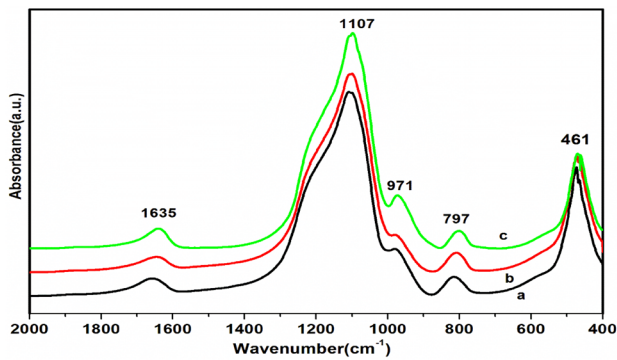
Fig. 3 FTIR spectra of **a** SMZL, **b** doped with 2 mol% Eu$_2$O$_3$ and **c** doped with 4 mol% of Eu$_2$O$_3$ ions nano-crystalline films
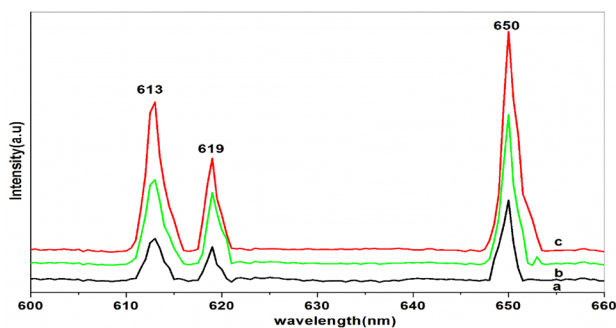

Fig. 4 PL spectra of **a** SMZL, **b** doped with 2 mol% Eu$_2$O$_3$ and **c** doped with 4 mol% of Eu$_2$O$_3$ ions nano-crystalline films

(SMZL) matrix are shown in Fig. 3, where the red emission band at 613 and 619 nm is ascribed to the $^5D_0$–$^7F_2$ transition [18]. The peaks in the red region from 610 to 660 nm with a maximum intense at ~650 nm were ascribed to $^5D_0$–$^7F_3$. It can be noticed that the good formation of the (SMZL) nano-crystalline changes the emission intensity of Eu^{3+} ions, due to the possible energy transfer behavior between Eu^{3+} and La$_2$O$_3$ NPs in (50 SiO$_2$-7MgO-20ZnO) [19, 20].

The produced PL emission band positions from 610 to 660 nm are attributed to Eu^{3+} ions in their local silicate network. This result is in agreement with that reported in the studies [19–21]

The prepared nano-crystalline films of SMZL doped with active Eu^{3+} ions have interesting photoluminescence

behavior. Due to the presence of three emission lines in the red regime of the energy transfer, these nano-materials might find multi-applications as waveguides, up converting and solar cells.

3.5 Density and molar volume

The estimated values of glass density (G_d) and molar volume (V_m) of the present (50 SiO$_2$:7 MgO: 20 ZnO: (23−x) La$_2$O$_3$−x Eu$_2$O$_3$) (SMZL) nano-porous films with different Eu$_2$O$_3$ amounts are listed in Table 1. The increment of Eu$_2$O$_3$ concentration leads to the increment of both G_d and V_m values. This would be expected due to the large values of the Eu$_2$O$_3$ density (G_d = 7.4 gm/cm^3) and molecular weight (351.93) in comparison with the other oxides [22].

3.6 Optical band gap

The experimental values of transmittance (T) and absorbance (A) for 50 SiO$_2$:7 MgO: 20 ZnO: (23−x) La$_2$O$_3$−x Eu$_2$O$_3$ nano-porous films were plotted versus the wavelength (λ) as shown in Fig. 5. Clearly, the Eu$_2$O$_3$ additions decrease the optical transmittance and shifts it to long wavelength range. This behavior corresponds to the internal transitions from the non-bridging bonds (NBO) in (SMZL) framework to covalently bond ((Si–O–Zn), (Si–O–Mg), and (Si–O–La)), which are bound with an excited electron from Eu^{3+} through oxygen bonds [10].

The absorption coefficient (α) is the most important optical constant that helps us to estimate the band gap (E_{opt}). It can be estimated directly from the absorbance by the following relationship: $\alpha = A/t$, where t is the film thickness. Incident photon energy ($h\upsilon$) dependence of the absorption index was described by Mott and Davis relation in the form of [23]:

$$\alpha = \frac{B(h\upsilon - E_{opt})^\partial}{h\upsilon} \tag{1}$$

where B is a constant and ∂ refers to the transition nature. The value of ∂ equals 1/2, 3/2, 2 or 3 corresponding to direct-allowed, direct-forbidden, indirect-allowed or indirect-forbidden, respectively. Semiconducting material was characterized by E_{opt} value between 0.0 and 4.0 eV. Figure 6

Table 1 Some physical parameters of (50)SiO$_2$ − 7MgO − 20ZnO − (23 − x)Li$_2$O − x Eu$_2$O$_3$ films

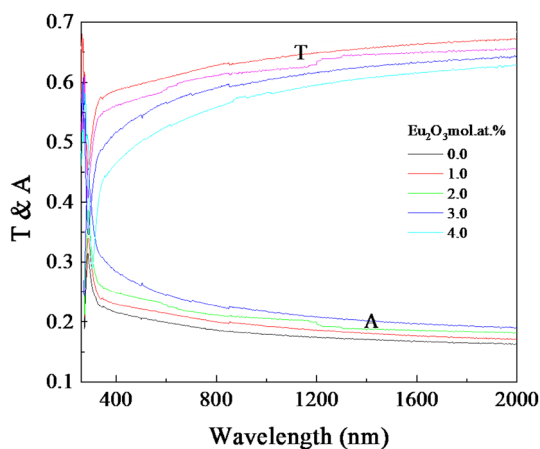| Eu$_2$O$_3$ mol%	Gd gm cm^{-3}	V_m cm^3	E_g eV	E_d eV	E_o eV	$n(0)$	$\varepsilon(0)$	$\alpha_{el}(0)$ cm^{-3}	$\Lambda(n(0))$	E_o/E_{opt}
0.0	2.62	21.07	2.38	23.23	4.22	2.55	6.51	3.00	1.17	1.77
1.0	2.65	21.93	2.31	25.10	4.15	2.65	7.04	3.20	1.21	1.80
2.0	2.74	22.81	2.23	27.86	4.10	2.79	7.79	3.43	1.25	1.84
3.0	2.77	24.15	2.15	29.87	4.03	2.90	8.41	3.71	1.29	1.88
4.0	2.86	24.42	2.03	33.20	4.02	3.04	9.26	3.84	1.30	1.98

Fig. 5 The T and A spectra of $(80 - x)SiO_2 - 11MgO - 9Li_2O - xEu_2O_3$ films
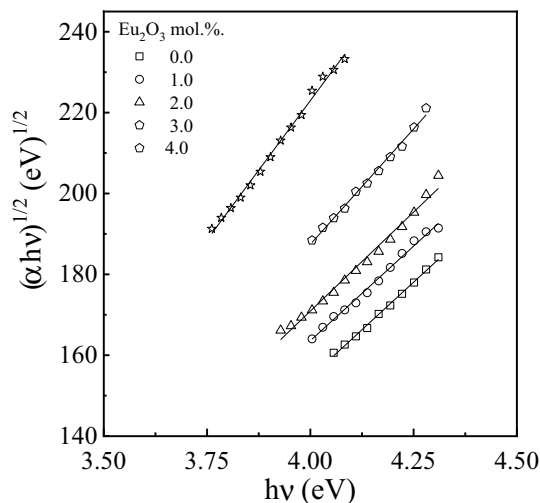

Fig. 6 $\sqrt{\alpha h\nu}$ opposite to the $h\nu$ for $(80 - x)SiO_2 - 11MgO - 9Li_2O - xEu_2O_3$ films

represents the plots of $\sqrt{\alpha h\nu}$ versus $h\nu$ for the 50 SiO$_2$:7 MgO: 20 ZnO: (23−x) La$_2$O$_3$−x Eu$_2$O$_3$ (SMZL) nano-porous films. The E_{opt} value was estimated as the intersect/slope ratio of Fig. 6. The E_{opt} values decrease with an increment of Eu$_2$O$_3$ content. This decrement in E_{opt} may be ascribed to the covalent behavior of the SMZL matrix which increases with increase in Eu$_2$O$_3$ concentration in the SMZL network.

3.6.1 Index of refraction and electronic polarizability

The index of refraction was estimated using the measured transmittance spectra through the following expression [24]:

$$n = \left(1 + \sqrt{(1 - T^2)}\right)/T \qquad (2)$$

The estimated values of index of refraction for the films under study were plotted against the wavelength as depicted in Fig. 7. As one can see, n decreases with extending λ which is a normal manner describing that n changes with λ values. On the other hand, the n values get incremented by increasing the Eu$_2$O$_3$ content. This manner can be explained by the increase in G_d, whereas both the n and G_d are correlated with each other through Eqs. [25–27]:

$$\alpha_{el} = \frac{\left[V_m\left((n^2 - 1)/(n^2 + 2)\right)\right] - \sum \alpha(cat)_i}{2.52N_o} \qquad (3)$$

where α_{el} is the electronic polarizability, $\sum \alpha(cat)_i$ is the molar cation polarizability. The $\sum \alpha(cat)_i$ and N_o are estimated as detailed here [25]. Figure 8 shows the spectral and compositional dependence of α_{el} for the studied films. It is clear that the polarizability increases with increasing Eu$_2$O$_3$ content which reflects the increase in n values. Here, the Si^{+4} ions with the lowest polarizability (0.033 A^3) and ionic radios (0.39 A) were replaced by Eu^{+3} ions with the largest polarizability (0.77 A^3) and ionic radios (1.31 A) [28]. The term $V_m\left((n^2 - 1)/(n^2 + 1)\right)$ is affected by the glass structure, namely the molar refraction (R_m), and is correlated with the molar electronic polarizability (α_m) through the relation: $\alpha_m = 3R_m/(4\pi N)$, where N is the number of Avogadro [28]. Figures 9 and 10 represent the variations in R_m and α_m values with the Eu$_2$O$_3$ content and/or λ for the SMZL nano-porous films. Obviously, both the R_m and α_m behave as α_{el} which is normal where R_m is directly proportional to both α_{el} and α_m.
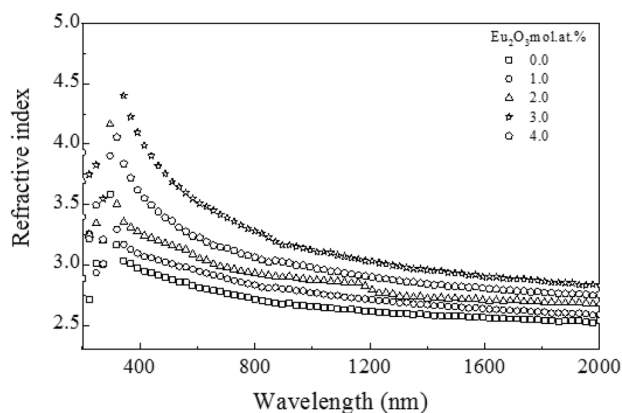

Fig. 7 The composition and wavelength dependence of n for $(80 - x)SiO_2 - 11MgO - 9Li_2O - xEu_2O_3$ films
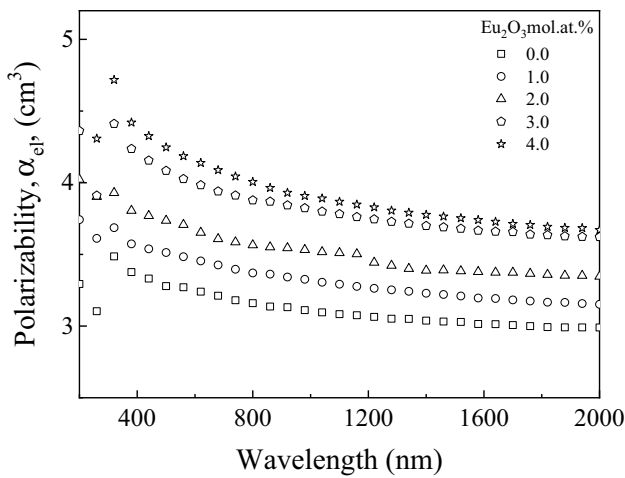
Fig. 8 The composition and wavelength dependence of α_{el} for $(80 - x)\text{SiO}_2 - 11\text{MgO} - 9\text{Li}_2\text{O} - x\text{Eu}_2\text{O}_3$ films
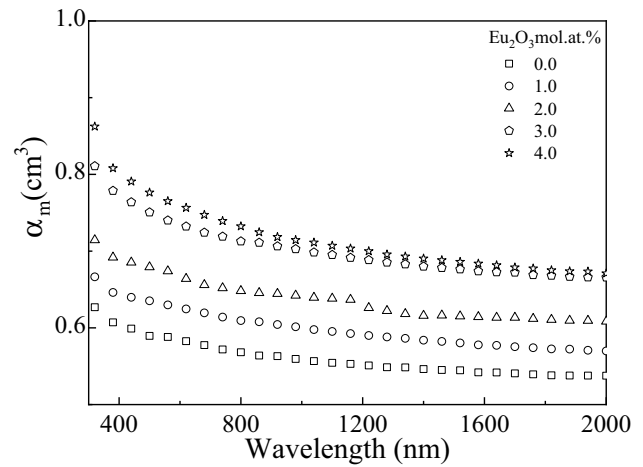

Fig. 10 The composition and wavelength dependence of α_m for $(80 - x)SiO_2 - 11MgO - 9Li_2O - xEu_2O_3$ films
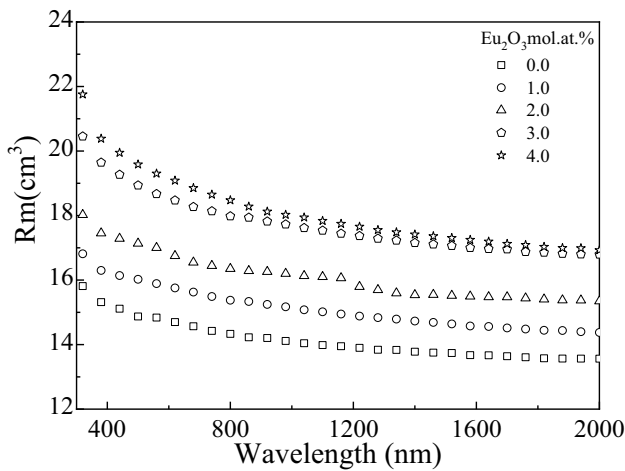

Fig. 9 The composition and wavelength dependence of R_m for $(80 - x)\text{SiO}_2 - 11\text{MgO} - 9\text{Li}_2\text{O} - x\text{Eu}_2\text{O}_3$ films
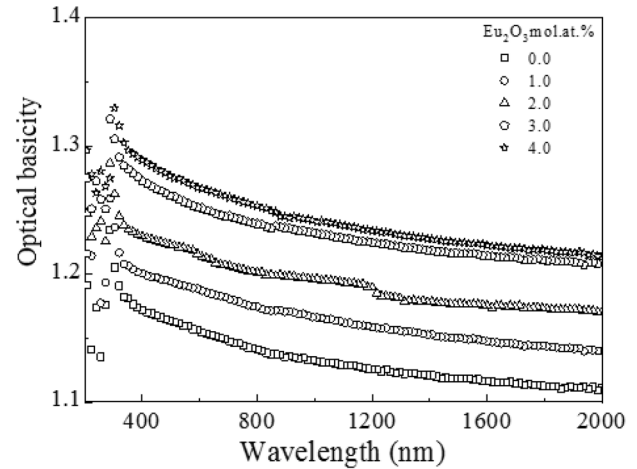

Fig. 11 The composition and wavelength dependence of $\Lambda(n)$ for $(80 - x)\text{SiO}_2 - 11\text{MgO} - 9\text{Li}_2\text{O} - x\text{Eu}_2\text{O}_3$ films

3.6.2 Optical basicity

Knowing the electronic polarizability helps one to estimate the optical basicity (Λ). The latter is a numerical expression of the average electron donor power of the oxide species constituting the medium, and it is a measure of the acid–base properties of oxides, glasses, alloys, slags, molten salts, etc. The relationship between the refractive index-based optical basicity $\Lambda(n)$ of the glass and the electronic polarizability (α_{el}) of the oxide ion in the structure is given by [29, 30]:

$$\Lambda(n) = \left(1.67\alpha_{el} - 1.67\right)/\alpha_{el} \tag{4}$$

The estimated values of the $\Lambda(n)$ are plotted as a function of λ and Eu_2O_3 content as represented in Fig. 11. The

observed increase in $\Lambda(n)$ suggests that the former oxides should be less basic compared with modifier oxides. The addition of modifier oxide to the former oxide results in the modification reaction to be acid–base reaction, in which the acidic region of former oxide is approached by modifier oxide ion in order to decrease acidities [31]. The increasing of optical basicity reflects the decrease in covalency. Based on the data, it indicates that the addition of modifier oxide reduces the acidity of the former oxide and increases the basicity of the glass.

3.6.3 Refractive index dispersion

As shown in Fig. 7, the index of refraction tends to a constant value at the transparent region. Here, one can apply
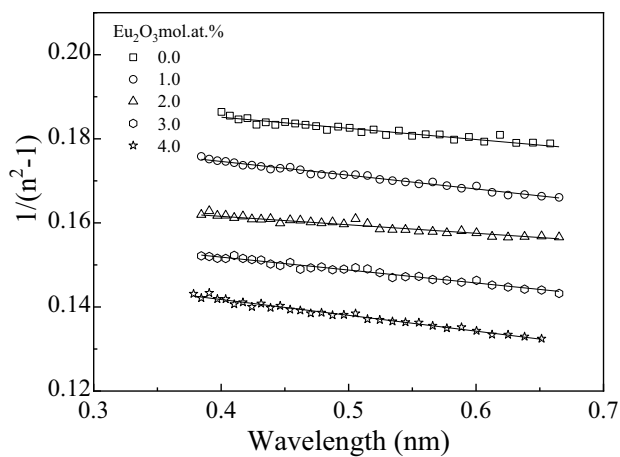
Fig. 12 $1/(n^2 - 1)$ vs. $h\nu$ for $(80 - x)\text{SiO}_2 - 11\text{MgO} - 9\text{Li}_2\text{O} - x\text{Eu}_2\text{O}_3$ films

the single oscillator model suggested by Wemple and Di-Domenico. In agreement with this model, the refractive index parameter $1/(n^2 - 1)$ is plotted against $h\nu$ as shown in Fig. 12. This figure represents the best fitting according to the following expression [30, 32, 33]:

$$\frac{1}{n^2 - 1} = \frac{E_o^2 - h\nu}{E_o E_d} \tag{5}$$

where E_o and E_d are the single oscillator and desperation energies, respectively. E_o and E_d values were estimated by using the slope and intersect of Fig. 12. The static index of refraction $n(0)$ is correlated with E_o, E_d and the static dielectric constant $(\varepsilon(0))$ through the two relations $n(0) = \sqrt{1 + E_d E_o^{-1}}$ and $\varepsilon(0) = n(0)^2$, respectively. E_o, E_d and $n(0)$ values are listed in Table 1. Both E_d and $n(0)$ values increase with increasing the amount of Eu$_2$O$_3$, whereas E_o decreases. The oscillating energy is an average energy gap ($E_{opt} \sim 0.5\ E_o$ (see Table 1)) [34]. The dispersion energy (E_d) is correlated with the effective coordination number of the cation nearest neighbor to the anion (N_c), the formal chemical valency of the anion (Z_a) and the effective number of valence electrons per anion (N_e) through this relation $\left(E_d = \beta Z_a N_c N_e \right)$, where β is a two-valued constant with either an ionic or a covalent value ($\beta_i = 0.26 \pm 0.03$ eV and $\beta_c = 0.37 \pm 0.04$ eV, respectively) [44, 45]. Substituting the value of $n(0)$ into Eqs. 3 and 4 gives the values of $\alpha_{el}(0)$ and $\Lambda(n(0))$ listed in Table 1.

4 Conclusions

Different films of the 50 SiO$_2$: 7MgO: 20 ZnO: $(23-x)$ La$_2$O$_3 - x$ Eu$_2$O$_3$ (SMZL) nano-porous films have been synthesized by the acidic sol–gel process. The film absorption

and index of refraction have been determined precisely based on the measured film transmittance and absorbance. The band gap E_{opt} decreases, whereas the index of refraction increases with the addition of Eu$_2$O$_3$ content. The obtained results were discussed considering structural changes, glass density, molar volume, electronic polarizability and optical basicity. Moreover, the Wemple–Di-Domenico model successfully describes the dispersion of the index of refraction. The photoluminescent results show three emission lines in the red regime of the energy transfer, so these nano-materials could be used as waveguides, up converting and solar cells.

References

1. J.L. Doualan, S. Girard, H. Haquin, J.L. Adam, J. Montagne, Opt. Mater. **24**(3), 563–574 (2003)
2. A. Biswas, G.S. Maciel, R. Kapoor, C.S. Friend, P.N. Prasad, Appl. Phys. Lett. **82**, 2389–2391 (2003)
3. I. Elgayar, A.E. Aliev, A.R. Boccaccini, R.G. Hill, J. Non-Cryst. Solids **351**(2), 173–183 (2005)
4. S.A. Lourenço, N.O. Dantas, E.O. Serqueira, W.E.F. Ayta, A.A. Andrade, M.C. Filadelpho, J.A. Sampaio, M.J.V. Bell, M.A. Pereira-da-Silva, J. Lumin. **131**(5), 850–855 (2011)
5. C.I. Merzbacher, W.B. White, J. Non-Cryst. Solids **130**(1), 18–34 (1991)
6. Amit Mallik, Arunabha Basumajumdar, P. Kundu, P. K. Maiti, Ceramics Int. **39**(3), 2551–2559 (2013)
7. R. Hill, J. Mater. Sci. Lett. **15**(13), 1122–1125 (1996)
8. A.M. ElNahrawy, A.B. AbouHammad, Int. J. Pharm. Tech. Res. **9**(8), 16–21 (2016)
9. M. Chatterjee, M.K. Naskar, Ceram. Int. **32**(6), 623–632 (2006)
10. A.M.E. Nahrawy, A.A. Moez, A.M. Saad, Silicon **10**(5), 2117–2122 (2018)
11. M. El Nahrawy Amany, A. M. Mansour, B. Abou Hammad Ali, R. Wassel Ahmed, Mater. Res. Express **6** (1), 016404 (2019)
12. A. M. Youssef, A. M. El-Nahrawy, A. B. Abou Hammad, Int. J. Biol. Macromol. **97** 561–567 (2017)
13. A.A. Elabd, O.A. Elhefnawy, A.M. El Nahrawy, RSC Adv. **6**(12), 9563–9570 (2016)
14. A. M. ElNahrawy, A. I. Ali, A. B. AbouHammad, A. AïchaMbarek, Egypt. J. Chem. **61**(6), 770–780 (2018)
15. M.M. ElOkr, F. Metawe, A.M. El-Nahrawy, B.A. Osman, Int. J. Chem. Tech. Res. **9**(5), 228–234 (2016)
16. S.P. Thompson, S.J. Day, J.E. Parker, A. Evans, C.C. Tang, J. Non-Cryst. Solids **358**(5), 885–892 (2012)
17. M. Abbas, B. P. Rao, Md. N. Islam, S. M. Naga, M. Takahashi, C. G. Kim, Ceram. Int. **40** (1, Part B), 1379–1385 (2014)
18. G. Li, Z. Wang, Yu. Min, Z. Quan, J. Lin, J. Solid State Chem. **179**(8), 2698–2706 (2006)
19. P. Mahata, S.K. Mondal, D.K. Singha, P. Majee, Dalton Trans. **46**, 301–328 (2017)
20. X. Li, H. Zhong, B. Chen, G. Sui, J. Sun, S. Xu, L. Cheng, J. Zhang, Opt. Express **26**, 1870–1881 (2018)
21. P. Chen, Y. Mao, S. Hou, Y. Chen, X. Liu, Y. Lou, A. Chen, L. Yang, J. Li, N. Dai, Ceram. Int. **45**, 233–238 (2019)

22. I. Bulus, M. Isah, M.E. Garba, R. Hussin, S.A. Dalhatu, Nigerian J. Technol. Dev. **15**(4), 121–127 (2018)

23. N.F. Mott, E.A. Davis, R.A. Street, Philos. Mag. **32**(5), 961–996 (1975)

24. R. Kaur, S. Singh, K. Singh, O.P. Pandey, Radiat. Phys. Chem. **86**, 23–30 (2013)

25. Y.B. Saddeek, E.R. Shaaban, E.S. Moustafa, H.M. Moustafa, Phys. B **403**(13–16), 2399–2407 (2008)

26. V. Dimitrov, T. Komatsu, J. Chem. Technol. Metal. **48**(6), 549–554 (2013)

27. K.A. Aly, J. Alloy Compd. **630**(1), 178–182 (2015)

28. V. Dimitrov, T. Komatsu, J. Univ. Chem. Technol. Metall. **45**(3), 219–250 (2010)

29. V. Dimitrov, T. Komatsu, J. Ceram. Soc. Jpn. **107**(10), 879–886 (1999)

30. K. A. Aly, Y. Saddeek, G. Abbady, S. R. Alharbi, J. Non-Cryst. Solids **475** (Supplement C), 161–166 (2017)

31. P. Chimalawong, J. Kaewkhao, C. Kedkaew, P. Limsuwan, J. Phys. Chem. Solids **71**(7), 965–970 (2010)

32. K.A. Aly, Appl. Phys. A Mater. Sci. Process **120**(1), 293–299 (2015)

33. M. Didomenico Jr., S.H. Wemple, Appl. Phys. Lett. **12**(10), 352–355 (1968)

34. K. Tanaka, Thin Solid Films **66**(3), 271–279 (1980)

Publisher's Note Springer Nature remains neutral with regard to jurisdictional claims in published maps and institutional affiliations.